Short-wave filter in Fourier representation of waves due to a steadily advancing ship hull

Francis Noblesse[1], **Fuxin Huang**[2], **Chi Yang**[2]

[1] David Taylor Model Basin, NSWC-CD, Bethesda MD, USA; noblfranc@gmail.com
[2] School of Physics, Astronomy & Computational Sciences, George Mason University, Fairfax VA, USA; fhuang@gmu.edu, cyang@gmu.edu

Abstract

The dual basic tasks of evaluating ship waves at the free surface and of removing unwanted short waves are considered within the framework of the 'free-surface Green function potential flow theory', based on a Green function that satisfies the radiation condition and the Kelvin-Michell linearized boundary condition at the free surface. A practical approach based on parabolic extrapolation within an extrapolation layer bordering the free surface is used. The height of the extrapolation layer is defined explicitly via simple analytical relations in terms of the Froude number and the slenderness of the ship hull, and varies from the bow to the stern. The bow-to-stern variation is an important ingredient that accounts for the fact that waves along the ship hull aft of the bow wave differ from the bow wave. Indeed, a ship bow wave is significantly higher and shorter than waves aft of the bow wave, is affected by nearfield effects related to the rapid variation of the hull geometry at a ship bow, and consequently contains more short wave components.

1 Introduction

An offshore structure (or any other floating body without mean forward speed) in ambient time-harmonic (regular) waves with frequency ω generates a system of (diffracted-radiated) waves that all have the same frequency ω and wavelength $\lambda = 2\pi g/\omega^2$. Such a system of waves, with a single *discrete* wavelength, differs in a fundamental respect from the waves — with a continuous spectrum of wavelengths — that are generated by a ship advancing in calm water or in ambient regular waves. In particular, for the simplest case of a ship advancing with forward speed V_s in calm water considered here, the ship creates waves with a spectrum of wavelengths λ within the range $0 \leq \lambda \leq 2\pi V_s^2/g$. Thus, ship waves defined within the classical framework of potential flow theory include very short waves that can be significantly affected by surface tension and viscosity, and consequently are physically unrealistic. The spectrum of ship waves may also include waves that are not appreciably affected by surface tension and viscosity but are short with respect to the ship length L_s, and consequently may have limited effect on the ship drag, sinkage and trim. There is then a practical need for eliminating short waves in the spectrum of waves generated by ships. Indeed, an effective and practical method for filtering short gravity waves is an important ingredient of any numerical method for computing ship waves. This basic issue is considered here within the framework of the 'free-surface Green function potential flow theory', based on a Green function that satisfies the radiation condition and the Kelvin-Michell linearized boundary condition at the free surface.

Thus, we consider linear potential flow about a ship hull of length L_s that steadily advances at speed V_s along a straight path in calm water of effectively infinite depth and lateral extent. The flow about the ship hull is observed from a righthanded moving system of orthogonal coordinates $\mathbf{X} \equiv (X, Y, Z)$ attached to the ship, and thus appears steady with flow velocity given by the sum of an apparent uniform current $(-V_s, 0, 0)$ opposing the ship speed V_s and the (disturbance) flow velocity $\mathbf{U} \equiv (U, V, W)$ due to the ship. The X axis is chosen along the path of the ship and points toward the ship bow. The Z axis is vertical and points upward, with the mean (undisturbed) free surface taken as the plane $Z = 0$. The length L_s and the speed V_s of the ship are used to define nondimensional coordinates $\mathbf{x} \equiv \mathbf{X}/L_s$ and flow potential $\phi \equiv \Phi/(V_s L_s)$.

We define the usual Froude number $F \equiv V_s/\sqrt{g L_s}$ where g is the acceleration of gravity. We also define the Froude number $F_{BD} \equiv V_s/\sqrt{g L^{BD}}$ based on a transverse dimension L^{BD} of the ship hull that is chosen as $L^{BD} \equiv BD/(B/2 + D)$. We have $L^{BD} < B$ and $L^{BD} < 2D$. The Foude numbers F and F_{BD} based on the length L_s or the transverse dimension L^{BD} of the ship are related as

$$F_{BD} \equiv \frac{F}{\sqrt{\sigma^H}} \quad \text{where} \quad \sigma^H \equiv \frac{L^{BD}}{L_s} \equiv \frac{b\,d}{b/2 + d} \quad \text{with} \quad b \equiv \frac{B}{L_s} \quad \text{and} \quad d \equiv \frac{D}{L_s} \tag{1}$$

For a beam/length ratio $b = 0.15$ and a draft/length ratio $d = 0.05$, the hull slenderness is $\sigma^H = 0.06$.

As already noted, the flow about the ship is considered within the framework of the 'free-surface Green function method' based on a Green function $G(\widetilde{\mathbf{x}}\,;\mathbf{x})$ that satisfies the radiation condition and the Kelvin-Michell linearized boundary condition at the free surface. The points $\mathbf{x} \equiv (x, y, z)$ and $\widetilde{\mathbf{x}} \equiv (\widetilde{x}, \widetilde{y}, \widetilde{z})$ stand for 'boundary points' located on the ship hull surface Σ^H, and 'flow-field points' located on Σ^H or in the flow region outside Σ^H.

Within this approach, the flow potential $\widetilde{\phi} \equiv \phi(\widetilde{\mathbf{x}})$ at a flow field point $\widetilde{\mathbf{x}}$ can be expressed as $\widetilde{\phi} = \widetilde{\phi}^L + \widetilde{\phi}^W$ where $\widetilde{\phi}^L$ represents a nonoscillatory local flow component and $\widetilde{\phi}^W$ defines the waves generated by the ship. These local and wave components are associated with the decomposition $G = L + W$ of the Green function G into a local flow component L and a wave component W, as in e.g. [1]. The local flow potential $\widetilde{\phi}^L$ is not considered here.

Thus, we only consider the wave potential $\widetilde{\phi}^W$. Within the free-surface Green function approach, the wave potential $\widetilde{\phi}^W \equiv \phi^W(\widetilde{\mathbf{x}})$ at a flow field point $\widetilde{\mathbf{x}} \equiv (\widetilde{x}, \widetilde{y}, \widetilde{z} \le 0)$ is expressed as a Fourier superposition of elementary plane waves $\widetilde{E}$. Specifically, $\widetilde{\phi}^W$ is given by

$$\widetilde{\phi}^W = \frac{1}{\pi}\,\Im\mathrm{m}\int_{-\infty}^{\infty} dk\,\widetilde{S}\,\widetilde{E} \quad \text{with} \quad \widetilde{E} \equiv\, e^{\,(1+k^2)\,\widetilde{z}\,/F^2 \,+\, i\,\sqrt{1+k^2}\,(\,\widetilde{x}\,+\,k\,\widetilde{y}\,)/F^2} \tag{2}$$

e.g. [2,3]. The amplitude $\widetilde{S} \equiv \widetilde{S}(k;\widetilde{x})$ of the elementary waves $\widetilde{E}$ in the Fourier representation (2), called wave-spectrum function or Kochin function, is also given by a Fourier superposition of elementary plane waves. Specifically, the wave-spectrum function $\widetilde{S}$ in (2) is given by a distribution of elementary waves E over the portion $\widetilde{\Sigma}^H$ of the mean wetted ship hull surface Σ^H that is defined by $\widetilde{x} \le x$. We then have

$$\widetilde{S} \equiv \frac{1}{F^2}\int_{\widetilde{\Sigma}^H} da\,A\,E \quad \text{with} \quad E \equiv\, e^{\,(1+k^2)\,z\,/F^2 \,-\, i\,\sqrt{1+k^2}\,(\,x\,+\,k\,y\,)/F^2} \tag{3}$$

Here, $da \equiv da(\mathbf{x})$ is the differential element of area at a point $\mathbf{x}$ of the ship hull surface Σ^H.

An important particular case of the generic Fourier-Kochin representation (2)-(3) of ship waves is the wave potential $\widetilde{\phi}^W_H$ associated with the Hogner slender-ship potential $\widetilde{\phi}_H$ given in [4]. In this special case, the amplitude A of the elementary wave E in the wave-spectrum function $\widetilde{S}$ is given by

$$A = A^H \quad \text{with} \quad A^H \equiv n^x \tag{4}$$

Here, $\mathbf{n} \equiv (n^x, n^y, n^z)$ is a unit vector that is normal to Σ^H at $\mathbf{x}$ and points outside Σ^H, i.e. into the water. The Hogner slender-ship approximation (4), defined explicitly in terms of the hull geometry, is useful for many practical applications. Furthermore, this explicit flow approximation is a major element of the Neumann-Michell (NM) theory of ship waves given in [3] and considered further on. Indeed, the NM theory provides a correction of the Hogner slender-ship potential $\widetilde{\phi}_H$ given in [4].

The wavelength λ of the elementary waves $\widetilde{E}$ and E in (2) and (3) is given by

$$0 \le \lambda \equiv 2\pi F^2/(1 + k^2) \le 2\pi F^2 \equiv \lambda_0 \tag{5a}$$

where λ_0 is the wavelength of the transverse waves generated by a ship along its track. Transverse and divergent ship waves correspond to $|k| < 1/\sqrt{2} \approx 0.71$ and $1/\sqrt{2} < |k|$, respectively; e.g. [5]. The ratio

$$\lambda/\lambda_0 = 1/(1 + k^2) \tag{5b}$$

is equal to 1/2 for $k = 1$, 1/3 for $k = \sqrt{2}$, 1/5 for $k = 2$, 1/10 for $k = 3$, and approximately 6% or 4% for $k = 4$ or $k = 5$. Thus, values of $|k|$ greater than 3 correspond to waves that are significantly shorter than the longest waves created by a ship.

The continuous spectrum of waves generated by a ship can be usefully divided into 'long waves' associated with the range $-k_{long} \le k \le k_{long}$ where the cutoff wavenumber k_{long} can reasonably be taken as 3 or even 2, and 'short waves' that correspond to $k_{long} \le |k|$. These short waves can be further divided into 'short gravity waves' that are too long to be significantly affected by surface tension and viscous effects, and 'very short waves' for which surface tension and viscous effects cannot be ignored. An elegant physics-based theory that accounts for the influence of surface tension and viscosity on gravity waves generated by a ship hull advancing in calm water or in ambient time-harmonic waves is expounded in [6-9]. Surface tension and viscosity are ignored here for simplicity, and because the cutoff wavenumber k_{long} is expected to correspond to relatively

long waves not significantly affected by surface tension and viscosity (although that may not always be the case at model scale).

For a fully submerged body, for which $z \le -\delta$ where $0 < \delta$ is the distance between the free surface plane $z = 0$ and the highest point of the submerged body surface (point nearest the mean free surface), we have $|E| \le e^{-(1+k^2)\,\delta/F^2}$. Thus, the elementary wave function E and consequently the spectrum function $\widetilde{S}$ decay exponentially as $k \to \pm\infty$ for a fully submerged body. The Fourier integral (2) therefore converges for every value of $\widetilde{z} \le 0$, and does not contain short waves, in this special case.

However, the situation is different, and more complicated, for a surface-piercing ship hull Σ^H, for which $z \le 0$ and the function E does not decay exponentially as $k \to \pm\infty$. If $\widetilde{z} \le -h < 0$, i.e. for flow field points $\widetilde{\mathbf{x}}$ at some distance below the mean free surface $\widetilde{z} = 0$, the exponential function $\widetilde{E}$ in (2) decays exponentially in the limit $k \to \pm\infty$ and the Fourier integral (2) can be evaluated accurately. In practice, the infinite limits of integration in (2) are replaced by finite limits $\pm k_\infty$. The function $\widetilde{E}$ is smaller than 0.7% if $(1+k^2)\,\widetilde{z}/F^2 < -5$, and (2) can be evaluated accurately for $\widetilde{z} \le -h_\infty$ with

$$h_\infty \equiv 5\,F^2/(1+k_\infty^2) \tag{6}$$

Convergence of the Fourier integral (2) is not a-priori obvious for $-h_\infty < \widetilde{z} \le 0$, i.e. for flow field points $\widetilde{\mathbf{x}}$ in the vicinity of the free surface $\widetilde{z} = 0$. Indeed, we have $\widetilde{E} = 1$ if $\widetilde{z} = 0$, for every value of the Fourier variable k.

Furthermore, the relation (6) yields $k_\infty \to \infty$ as $h_\infty \to 0$, and therefore implies that the wave potential $\widetilde{\phi}^W$ includes very short waves in this limit. However, very short gravity waves are unrealistic because surface tension and viscous effects, ignored in (2) and (3), cannot be neglected in the short-wave limit $k \to \infty$, and because short waves that correspond to $k_{long} \le |k|$ are of limited interest for most practical applications. Thus, robust evaluation of the wave integral (2) for $-h_\infty < \widetilde{z} \le 0$ is a nontrivial basic issue for the computation of ship waves within the framework of the free-surface Green function approach.

A practical way of evaluating the Fourier integral (2) at and near the mean free surface $\widetilde{z} = 0$ is then required. To this end, the Fourier representation (2) can be modified as

$$\widetilde{\phi}^W = \frac{1}{\pi}\,\Im\mathrm{m}\int_{-k_\infty}^{k_\infty} dk\,\Lambda\,\widetilde{S}\,\widetilde{E} \tag{7}$$

Selection of an appropriate finite limit of integration (cut-off wavenumber) k_∞, and an effective short-wave filter function Λ are important elements of the free-surface Green function theory of ship waves as already noted.

2 Parabolic extrapolation

A simple way of evaluating the Fourier integral (2) for flow-field points $\widetilde{\mathbf{x}}$ within a layer $-\widetilde{h} \le \widetilde{z} \le 0$ near the mean free-surface plane $\widetilde{z} = 0$ is via extrapolation of the wave potential $\widetilde{\phi}^W$ computed at points $\widetilde{\mathbf{x}}$ in the region $\widetilde{z} \le -\widetilde{h}$. In particular, the wave potential $\widetilde{\phi}_0^W$ at a point $\widetilde{\mathbf{x}}_0$ of the mean free surface, i.e. with $\widetilde{z}_0 = 0$, can be determined via parabolic extrapolation of the wave potentials $\widetilde{\phi}_1^W$, $\widetilde{\phi}_2^W$, $\widetilde{\phi}_3^W$ computed at three points $\widetilde{\mathbf{x}}_1$, $\widetilde{\mathbf{x}}_2$, $\widetilde{\mathbf{x}}_3$ with $\widetilde{z}_3 < \widetilde{z}_2 < \widetilde{z}_1 \le -\widetilde{h}$. Specifically, the parabolic approximation

$$\widetilde{\phi}^W \approx \frac{(\widetilde{z}-\widetilde{z}_2)(\widetilde{z}-\widetilde{z}_3)\,\widetilde{\phi}_1^W}{(\widetilde{z}_1-\widetilde{z}_2)(\widetilde{z}_1-\widetilde{z}_3)} + \frac{(\widetilde{z}-\widetilde{z}_1)(\widetilde{z}-\widetilde{z}_3)\,\widetilde{\phi}_2^W}{(\widetilde{z}_2-\widetilde{z}_1)(\widetilde{z}_2-\widetilde{z}_3)} + \frac{(\widetilde{z}-\widetilde{z}_1)(\widetilde{z}-\widetilde{z}_2)\,\widetilde{\phi}_3^W}{(\widetilde{z}_3-\widetilde{z}_1)(\widetilde{z}_3-\widetilde{z}_2)}$$

with $\widetilde{z} = 0$ yields the extrapolation formula

$$\widetilde{\phi}_0^W \approx 3\,(\widetilde{\phi}_1^W - \widetilde{\phi}_2^W) + \widetilde{\phi}_3^W \quad \text{if} \quad \widetilde{z}_1 \equiv -\widetilde{h}, \widetilde{z}_2 \equiv -2\widetilde{h}, \widetilde{z}_3 \equiv -3\widetilde{h}$$

This parabolic extrapolation formula amounts to replacing the exponential function $\widetilde{E} \equiv e^{\,(1+k^2)\,\widetilde{z}/F^2}$ in (2) by the function

$$\widetilde{E}_0 \equiv \widetilde{E}_h\,(3 - 3\,\widetilde{E}_h + \widetilde{E}_h^2) \quad \text{with} \quad \widetilde{E}_h \equiv e^{-(1+k^2)\,\widetilde{h}/F^2}$$

for $\widetilde{z} = 0$. We have $\widetilde{E}_h \to 0$ and $\widetilde{E}_0 \sim 3\,\widetilde{E}_h$ as $k \to \pm\infty$. Thus, while $\widetilde{E} = 1$ for $\widetilde{z} = 0$, $\widetilde{E}_0$ vanishes in the limit $k \to \pm\infty$. The function $\widetilde{E}_*$ defined as

$$\widetilde{E}_* \equiv \widetilde{E}_0\,(1 + \widetilde{z}/\widetilde{h}) - \widetilde{E}_h\,\widetilde{z}/\widetilde{h} \equiv \widetilde{E}_h\,[3 - 3\,\widetilde{E}_h + \widetilde{E}_h^2 + (2 - 3\,\widetilde{E}_h + \widetilde{E}_h^2)\,\widetilde{z}/\widetilde{h}\,] \qquad \text{with} \quad -\widetilde{h} \le \widetilde{z} \le 0$$

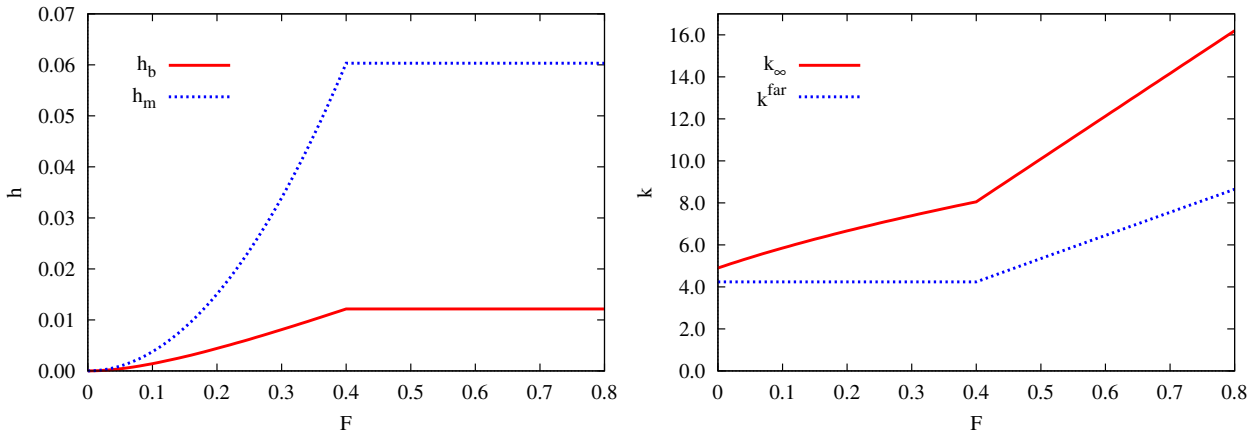

Figure 1: Variations of the midship and bow-wave extrapolation heights h_m and h_b (left side) and of the cutoff wavenumbers k_∞ and $k^{\rm far}$ (right side) within the range $0 \le F \le 0.8$ for $F_t = 0.4$, $\sigma^H = 0.06$, $\varepsilon_b = 0.04$, $\varepsilon_m = 0.06$ and $C_s^m = 0.7$.

can be substituted for the function $\widetilde{E}$ within the layer $-\widetilde{h} \le \widetilde{z} \le 0$ near the free surface $\widetilde{z} = 0$. The wave potential $\widetilde{\phi}^W$ is not affected for $\widetilde{z} \le -\widetilde{h}$ if the exponential function $\widetilde{E}$ in the Fourier integral (2) is replaced by the function $\widetilde{E}_* \equiv \Lambda\,\widetilde{E}$ where the function Λ is defined as

$$\left\{\begin{array}{l} \Lambda \equiv 1 \quad \text{for} \;\; \widetilde{z} \le -\widetilde{h} \\ \Lambda \equiv \; e^{-\,(1+k^2)\,(\widetilde{h}+\widetilde{z})/F^2}\,[3 - 3\,\widetilde{E}_h + \widetilde{E}_h^2 + (2 - 3\,\widetilde{E}_h + \widetilde{E}_h^2)\,\widetilde{z}/\widetilde{h}\,] \quad \text{for} \;\; -\widetilde{h} \le \widetilde{z} \le 0 \\ \qquad \text{with} \quad \widetilde{E}_h \equiv e^{-(1+k^2)\,\widetilde{h}\,/F^2} \end{array}\right\} \tag{8}$$

The replacement of the function $\widetilde{E}$ in (2) by the function $\widetilde{E}_* \equiv \Lambda\,\widetilde{E}$ amounts to multiplying the integrand of the Fourier integral (2) by the function Λ, as in (7). This function provides a reasonable extension of the wave potential $\widetilde{\phi}^W$ (which is unaffected for $\widetilde{z} \le -\widetilde{h}$) up to the free surface $\widetilde{z} = 0$, and ensures convergence of the Fourier integral (7). The function Λ and the finite limits of integration $\pm k_\infty$ act as a filter that eliminates short waves in (2).

The short-wave filter (8) depends on $\widetilde{z}/F^2$ and $\widetilde{h}/F^2$. Furthermore, the 'extrapolation height' $\widetilde{h}$ of the 'extrapolation layer' $-\widetilde{h} < \widetilde{z} \le 0$ can (indeed, should) be chosen to vary with $\widetilde{x}$, as shown below. The filter (8) is more elaborate than the simpler filter used in [2,10], which is independent of $\widetilde{x}$ and $\widetilde{z}$. The filter (8) is also more effective, notably because an extrapolation height $\widetilde{h}$ that varies along the length of a ship hull is useful as now shown.

3 Basic extrapolation heights and related cutoff wavenumbers

Waves along a ship hull at midship — at some distance away from the ship bow and stern where the hull geometry varies rapidly — are largely determined by the ship speed. Indeed, 'midship waves' have a wavelength approximately equal to the (nondimensional) wavelength $\lambda_0 \equiv 2\pi F^2$ of the longest waves generated by a ship along its track. The fundamental wavelength λ_0 is approximately equal to 1 (the nondimensional ship length) for $F \approx 0.4$. The extrapolation height $\widetilde{h}$ for the waves along a ship hull at midship (aft of the bow wave and ahead of the ship stern) can then be taken as a small fraction $0 < \varepsilon_m \ll 1$ of the longest wavelength λ_0, i.e. $h_m = \varepsilon_m\,2\pi F^2$. This extrapolation height increases rapidly as the Froude number F increases, and ultimately becomes meaningless. Indeed, at high Froude numbers, the waves generated by a ship are increasingly influenced by the variation of the hull geometry, which is primarily determined by the hull slenderness σ^H defined by (1). The extrapolation height h_m can then be assumed to be proportional to σ^H, i.e. $h_m = C_m^H\,\sigma^H$, in the high Froude number limit. Thus, the 'midship extrapolation height' h_m is taken as

$$h_m = \min(\varepsilon_m\,2\pi F^2, C_m^H\,\sigma^H) \tag{9a}$$

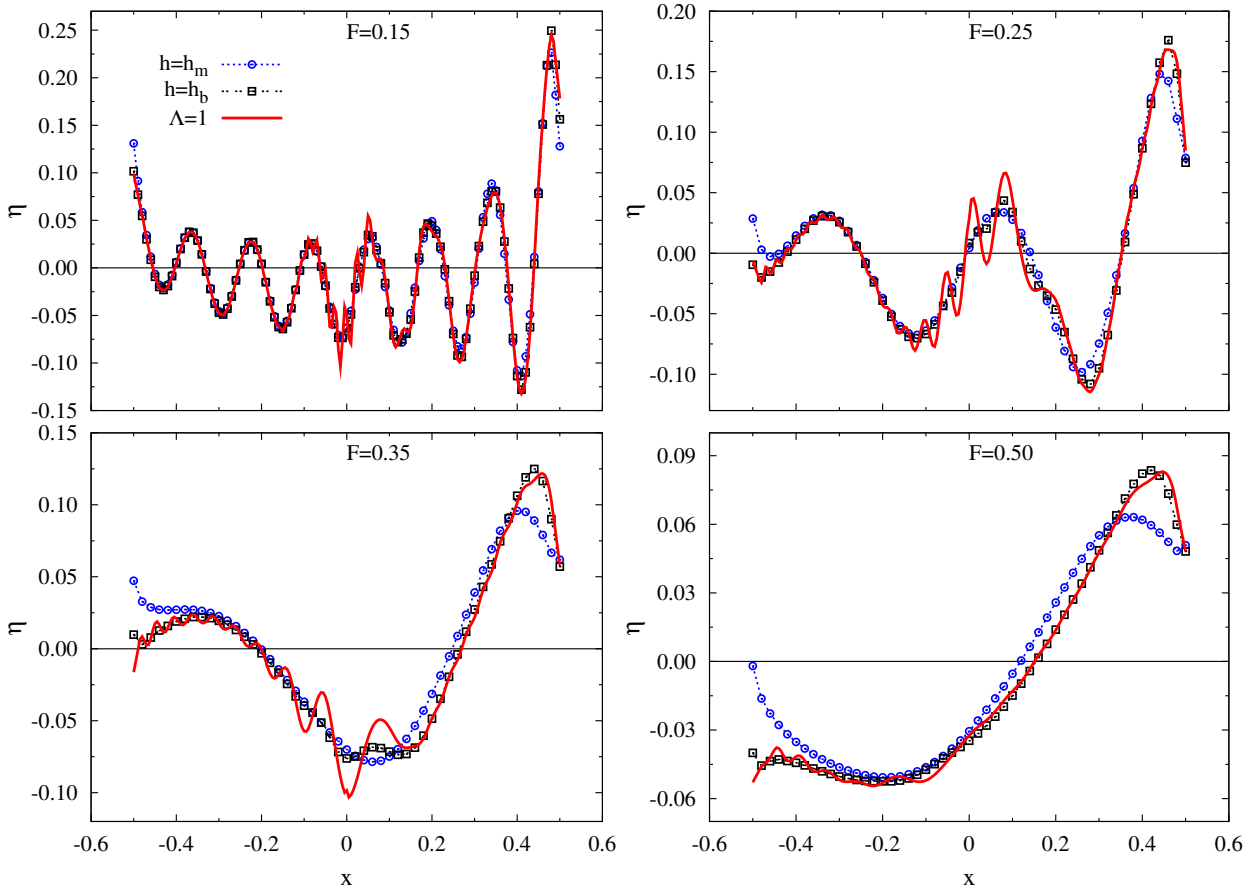

Figure 2: Wave profiles, predicted by Hogner's slender-ship approximation, along the Wigley hull at four Froude numbers $F = 0.15,\ 0.25,\ 0.35$ and 0.5. The curves marked $h = h_m$ or $h = h_b$ correspond to an extrapolation height $\widetilde{h}$ that is constant for $-0.5 \le \widetilde{x} \le 0.5$ and equal to the basic extrapolation heights h_m or h_b defined by (10a). The curves marked $\Lambda = 1$ correspond to k_∞ given by (11) and $\Lambda = 1$ (no parabolic filter) in (7).

We then have $h_m = \varepsilon_m 2\pi F^2$ or $h_m = C_m^H \sigma^H$ for $F \le F_m$ or $F_m \le F$ where the transition Froude number F_m between the low-speed and high-speed regimes is given by

$$F_m \equiv \sqrt{\frac{C_m^H \sigma^H}{2\pi \varepsilon_m}}$$

Numerical tests for the Wigley hull show that the physically reasonable choices $\varepsilon_m \approx 0.06$ and $C_m^H \approx 1$ are satisfactory. These values of ε_m and C_m^H yield a transition Froude number $F_m \approx 0.4$ (for which we have $\lambda_0 \approx 1$) for a typical hull slenderness $\sigma^H = 0.06$.

Ship bow waves and stern waves — in the vicinity of a ship bow and stern where the hull geometry varies rapidly — differ significantly from a transverse wave with wavelength approximately equal to λ_0. In particular, a ship bow wave is significantly shorter, higher, and consequently sharper than waves along a ship hull aft of the bow wave. A ship bow wave also contains more short divergent waves and is more directly affected by the hull geometry, specifically the shape of the ship bow. Indeed, a ship bow wave is strongly affected by nearfield effects associated with a sudden change of flow direction at a ship bow; [11]. In particular, while waves along a ship hull aft of the ship bow are nearly sinusoidal, with wavelength approximately equal to λ_0 as already noted, the portion of the wave profile between a ship stem and the crest of the bow wave, i.e. the bow wave front, is well approximated by a parabola [11,12]. The base of this parabola, i.e. the (nondimensional) distance $\ell_{front} \equiv L_{front}/L_s$ from the ship stem to the $x-$location of the bow wave crest, is shown in [11,13] to be approximately given by

$$\ell_{front} = CF^2/(1+V_s/\sqrt{gD}) \approx CF^2/(1+F_{BD}) \equiv CF^2/(1+F/\sqrt{\sigma^H})$$

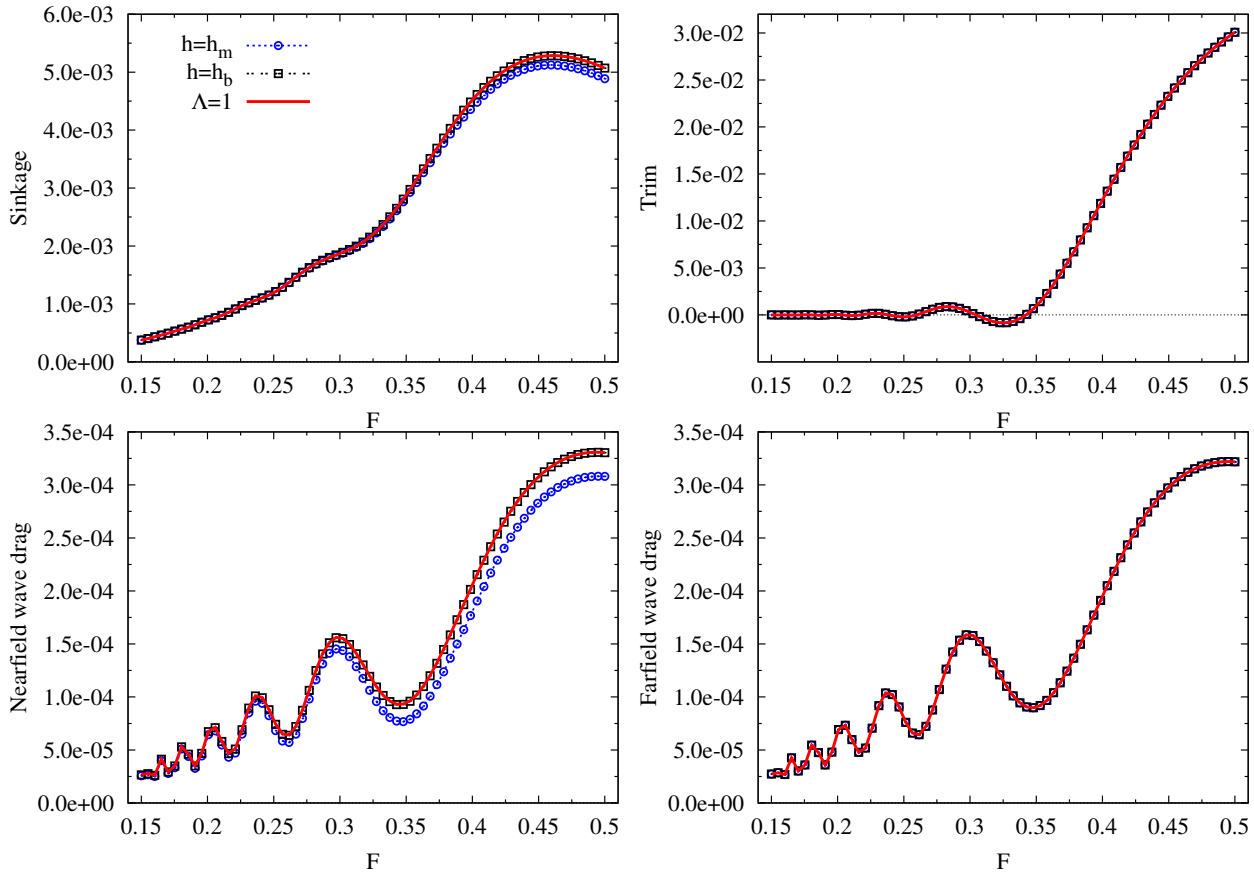

Figure 3: Sinkage (top left corner), trim (top right), nearfield drag (bottom left) and farfield drag (bottom right) predicted by Hogner's slender-ship approximation for the Wigley hull in the range $0.15 \le F \le 0.5$. The curves marked $h = h_m$ or $h = h_b$ correspond to an extrapolation height $\widetilde{h}$ that is constant for $-0.5 \le \widetilde{x} \le 0.5$ and equal to the basic extrapolation heights h_m or h_b defined by (10a). The curves marked $\Lambda = 1$ correspond to k_∞ given by (11) and $\Lambda = 1$ (no parabolic filter) in (7).

with a proportionality factor $C \approx 1.1$ for a wedged shaped bow. F_{BD} is the Froude number (1) associated with the characteristic transverse dimension L^{BD}, which is used here instead of the ship draft D. Thus, ℓ_{front} is $O(F^2)$ as $F \to 0$ and $O(F)$ as $F \to \infty$. An effective wavelength λ^{bow} that approximately corresponds to the length ℓ_{front} of the front of the bow wave can be taken as $C' \ell_{front}$ with a proportionality factor $4 \le C' \le 5$. The extrapolation height h_b related to the filtering of short waves at a ship bow is taken as a small fraction $0 < \varepsilon_b \ll 1$ of the effective bow wavelength λ^{bow}. Thus, h_b is chosen as $h_b \equiv C_* \varepsilon_b F^2/(1 + F/\sqrt{\sigma^H})$ with $C_* \equiv C'C \approx 5$. The value $C_* = 5$ is used here. This expression for the extrapolation height h_b becomes meaningless at high Froude numbers, as already noted. Indeed, as for the 'midship extrapolation height' h_m, the 'bow-wave extrapolation height' h_b can be assumed to be proportional to σ^H, i.e. $h_b \equiv C_b^H \sigma^H$, in the high Froude number limit. Thus, h_b is taken as

$$h_b \equiv \min\left(\frac{5\,\varepsilon_b F^2}{1 + F/\sqrt{\sigma^H}} \,,\, C_b^H \sigma^H \right) \tag{9b}$$

The transition Froude number F_b between the low-speed and high-speed regimes is given by

$$F_b \equiv \frac{C_b^H \sqrt{\sigma^H}}{10\,\varepsilon_b} \left(1 + \sqrt{1 + 20\,\varepsilon_b / C_b^H} \right)$$

Numerical tests for the Wigley hull show that the physically reasonable choices $\varepsilon_b \approx 0.04$ and $C_b^H \approx 0.2$ are satisfactory. These values of ε_b and C_b^H yield a transition Froude number $F_b \approx 0.4$ for a typical hull slenderness $\sigma^H = 0.06$.

The transition Froude numbers $F_m \approx 0.4$ and $F_b \approx 0.4$ are consistent. These transition Froude numbers

are strictly equal if

$$8\,\pi\,\varepsilon_m\,/C_m^H = A_b^2\,/(1+\sqrt{1+A_b})^2 \quad \text{with} \quad A_b \equiv 20\,\varepsilon_b\,/C_b^H$$

This relation yields $C_m^H \approx 1$ for $\varepsilon_m = 0.06$, $\varepsilon_b = 0.04$ and $C_b^H = 0.2$.

Alternatively, the midship and bow-wave extrapolation heights h_m and h_b can be expressed as

$$h_m \equiv 2\,\pi\,\varepsilon_m \min(F^2, F_t^2) \qquad\qquad h_b \equiv 5\,\varepsilon_b \min\left(\frac{F^2}{1+F/\sqrt{\sigma^H}}\,,\,\frac{F_t^2}{1+F_t/\sqrt{\sigma^H}}\right) \tag{10a}$$

As already noted, numerical tests for the Wigley hull show that $F_t \approx 0.4$, $\varepsilon_m \approx 0.06$ and $\varepsilon_b \approx 0.04$ are satisfactory choices, and expressions (10a) are then used here with $F_t = 0.4$, $\varepsilon_m = 0.06$ and $\varepsilon_b = 0.04$.

The hull geometry near the ship stern typically varies rapidly, as in the bow region. Thus, we can expect that the extrapolation height $\widetilde{h}$ should decrease near the stern, as in the bow region. However, the wave generated by a ship stern is not as well understood as the bow wave — for which considerable information is known, e.g. [11-14] — and is more complicated due to viscous effects. For lack of greater knowledge, the 'stern extrapolation height' h_s is then simply taken proportional to the midship extrapolation height h_m, i.e.

$$h_s = C_s^m\,h_m \tag{10b}$$

Numerical tests for the Wigley hull show that $C_s^m = 0.7$ is a reasonable choice. However, for a ship hull with a transom stern for which the flow extends smoothly aft of the transom, the geometry of the ship hull surface and related wake model aft of the transom does not vary rapidly near the stern, and the choice $C_s^m \approx 1$ is appropriate.

Expressions (10a) and (10b) yield $h_b \le \widetilde{h}$. Thus, h_∞ in (6) and the related cutoff wavenumber k_∞ in (7) can be taken as $h_\infty = h_b$ and $k_\infty = \sqrt{5\,F^2/h_b - 1}$ with h_b given by (10a). We then have

$$k_\infty = \sqrt{\frac{1-\varepsilon_b + F/\sqrt{\sigma^H}}{\varepsilon_b}} \quad \text{if } F \le F_t \qquad\qquad k_\infty = \frac{F}{F_t}\sqrt{\frac{1+F_t/\sqrt{\sigma^H} - \varepsilon_b F_t^2/F^2}{\varepsilon_b}} \quad \text{if } F_t \le F \tag{11}$$

These relations show that k_∞ increases with respect to the Froude number F, approximately in proportion to F or $\sqrt{F}$ in the high-speed or low-speed regimes $F_t \le F$ and $F \le F_t$, respectively. The smallest value of k_∞, attained in the limit $F = 0$, is $\sqrt{1-\varepsilon_b}/\sqrt{\varepsilon_b} \approx 1/\sqrt{\varepsilon_b}$. We then have $5 \le k_\infty$ for $\varepsilon_b = 0.04$.

The nondimensional wave drag coefficient $C_{\text{wave}} \equiv D_{\text{wave}}/(\rho\,V_s^2 L_s^2)$ that is associated with the energy transported by the farfield waves is determined in terms of the 'farfield' wave spectrum function $\widetilde{S}^{\text{far}} \equiv \widetilde{S}(k;\widetilde{x}=x_s)$ evaluated at the ship stern $\widetilde{x} = x_s$. Specifically, the farfield wave drag coefficient $C_{\text{wave}}^{\text{far}}$ is defined by the classic Havelock formula as

$$C_{\text{wave}}^{\text{far}} = \frac{1}{2\,\pi}\int_{-k^{\text{far}}}^{k^{\text{far}}} dk\; e^{-5\,(k/k^{\text{far}})^4}\sqrt{1+k^2}\,(S_{\text{r}}^2 + S_{\text{i}}^2) \quad \text{with} \quad S_{\text{r}} \equiv \text{Re}(S^{\text{far}}) \quad S_{\text{i}} \equiv \text{Im}(S^{\text{far}}) \tag{12}$$

where the filter function $e^{-5\,(k/k^{\text{far}})^4}$ is inserted to ensure more robust convergence. The truncation wavenumber k^{far} is related to the wave spectrum function at the ship stern $\widetilde{x} = x_s$ as already noted, and can then be taken as $k^{\text{far}} = \sqrt{5\,F^2/h_s - 1}$. Expressions (10a) and (10b) yield

$$k^{\text{far}} = \sqrt{\frac{2.5/\pi}{C_s^m\,\varepsilon_m} - 1} \quad \text{if } F \le F_t \qquad\qquad k^{\text{far}} = \frac{F}{F_t}\sqrt{\frac{2.5/\pi}{C_s^m\,\varepsilon_m} - \frac{F_t^2}{F^2}} \quad \text{if } F_t \le F \tag{13}$$

These relations show that k^{far} is independent of the Froude number (approximately equal to 4.2 for $\varepsilon_m = 0.06$ and $C_s^m = 0.7$) in the low-speed regime $F \le F_t$, and increases approximately in proportion to F in the high-speed regime $F_t \le F$. The low-speed relation (13) is consistent with the relation given in [3] .

The variations of the midship and bow-wave extrapolation heights h_m and h_b and of the cutoff wavenumbers k_∞ and k^{far} with respect to the Froude number F within the range $0 \le F \le 0.8$ are depicted on the left and right sides of Fig.1, respectively, for $F_t = 0.4$, $\sigma^H = 0.06$, $\varepsilon_b = 0.04$, $\varepsilon_m = 0.06$ and $C_s^m = 0.7$.

For illustration purposes, the Hogner slender-ship approximation is considered for the classic Wigley parabolic hull. Fig.2 depicts wave profiles along the Wigley hull at four Froude numbers $F = 0.15$, 0.25, 0.35 and 0.5. Three cases are considered in Fig.2. Two of the cases, marked $h = h_m$ or $h = h_b$, correspond to an extrapolation height $\widetilde{h}$ that is constant for $-0.5 \le \widetilde{x} \le 0.5$ and equal to the basic extrapolation heights h_m

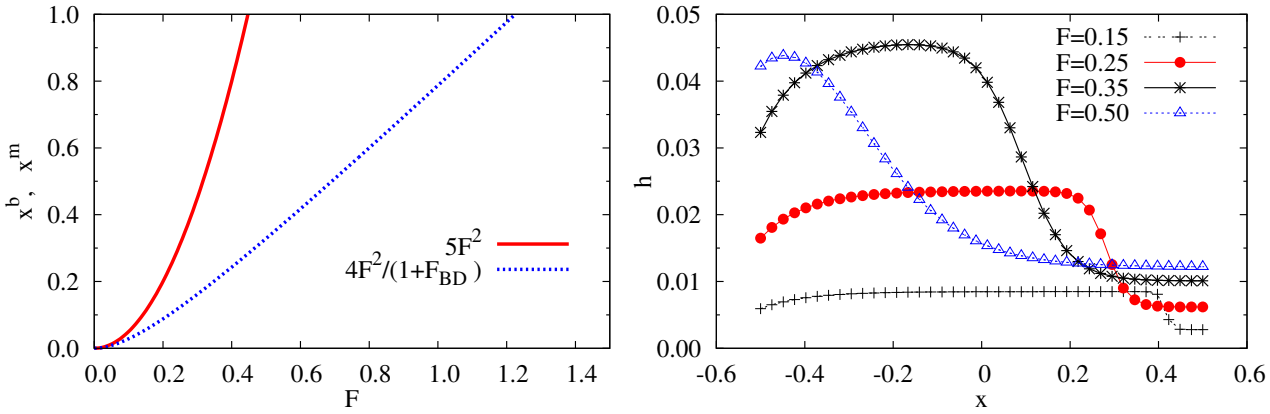

Figure 4: The left side depicts the functions $x^m \equiv \mu_m F^2$ and $x^b \equiv \mu_b F^2/(1+F_{BD})$ with $\mu_m = 5$, $\mu_b = 4$ and $\sigma^H = 0.06$. The right side depicts the variation of the extrapolation height $\widetilde{h}(\widetilde{x})$ defined by (14a)-(14d) with (10a) and (10b) for $F = 0.15$, 0.25, 0.35, 0.5 and $F_t = 0.4$, $\sigma^H = 0.06$, $\varepsilon_b = 0.04$, $\mu_b = 4$, $\mu_m = 5$, $\varepsilon_m = 0.06$, $C_s^m = 0.7$ and $\ell_s = 0.4$.

or h_b defined by (10a). The third case in Fig.2, marked $\Lambda = 1$, corresponds to k_∞ given by (11) and $\Lambda = 1$ (parabolic filter turned off) in (7). Thus, the cutoff wavenumber k_∞ is the same for the curves marked $h = h_b$ or $\Lambda = 1$, and differences between these curves illustrate both the practical necessity of removing short waves and the effectiveness of the parabolic filter (8) and the related filter function Λ in the Fourier integral (7). The wave profiles obtained using $h = h_m$ or $h = h_b$ differ significantly. In particular, the choice $h = h_m$ yields significantly lower bow waves than the choice $h = h_b$, in accordance with the property that a ship bow wave is shorter, higher, and more influenced by short waves and nearfield effects associated with the rapid variation of the hull geometry at the bow, than waves aft of a bow wave. Differences between the curves $h = h_m$ or $h = h_b$ are significant also aft of the bow wave, notably near the ship stern $\widetilde{x} = -1/2$ and at high Froude numbers. In particular, the curves $h = h_b$ contain oscillations (most clearly apparent for $F = 0.25$ and $F = 0.35$) that do not appear in the curves $h = h_m$. The differences between the curves marked $h = h_m$ or $h = h_b$ illustrate that $h = h_b$ or $h = h_m$ are better choices for a bow wave or waves aft of a bow wave, respectively, as already explained.

Fig.3 shows the sinkage and trim (top left and right corners), and the nearfield and farfield wave drags (bottom left and right corners) — obtained via integration of the pressure at the hull surface or the Havelock formula (12), respectively — for $0.15 \le F \le 0.5$, that correspond to the curves marked $h = h_m$, $h = h_b$ or $\Lambda = 1$ considered in Fig.2. The nondimensional sinkage, trim, and wave drag depicted in Fig.3, and in subsequent figures, are defined as in [3]. The extrapolation heights $h = h_m$ or $h = h_b$ yield nearly identical predictions of trim and farfield drag. For the sinkage (top left corner), differences between the curves $h = h_m$ or $h = h_b$ are small, and increase as the Froude number F increases. Differences for the nearfield drag (bottom left corner) are also relatively small, although larger, and likewise increase as F increases. The choice $h = h_m$ yields a lower nearfield drag than the choice $h = h_b$, in accordance with the property illustrated in Fig.2 that $h = h_m$ yields a lower bow wave than $h = h_b$. Whereas Fig.2 shows relatively large differences between the wave profiles for $h = h_b$ or $\Lambda = 1$, the curves $h = h_b$ or $\Lambda = 1$ in Fig.3 can hardly be distinguished. This result justifies the removal of short waves. Indeed, short waves have much smaller effect on integrated flow quantities (sinkage, trim and wave drag) of greatest practical importance than on the wave profiles along the ship hull and the pressure distribution at the hull.

4 Bow-to-stern variation of extrapolation height

The foregoing analysis shows that the extrapolation height $\widetilde{h}$ in (8) should be allowed to vary along the ship hull. The variation of $\widetilde{h}$ along the hull is then taken as

$$\widetilde{h} = h_m - (h_m - h_b)B_b(\widetilde{x}) - (h_{mb} - h_s)B_s(\widetilde{x}) \quad \text{with} \quad h_{mb} \equiv h_m - (h_m - h_b)B_b(\widetilde{x} = -1/2) \tag{14a}$$

The functions $B_b(\widetilde{x})$ and $B_s(\widetilde{x})$ are equal to 1 at the bow $\widetilde{x} = 1/2$ or the stern $\widetilde{x} = -1/2$, respectively. The length of the bow region where we have $B_b \approx 1$ is related to the distance $\ell_{front} \approx F^2/(1+F_{BD})$ between the ship stem and the crest of the bow wave, which defines the front of the bow wave. We then impose $B_b \approx 1$ for

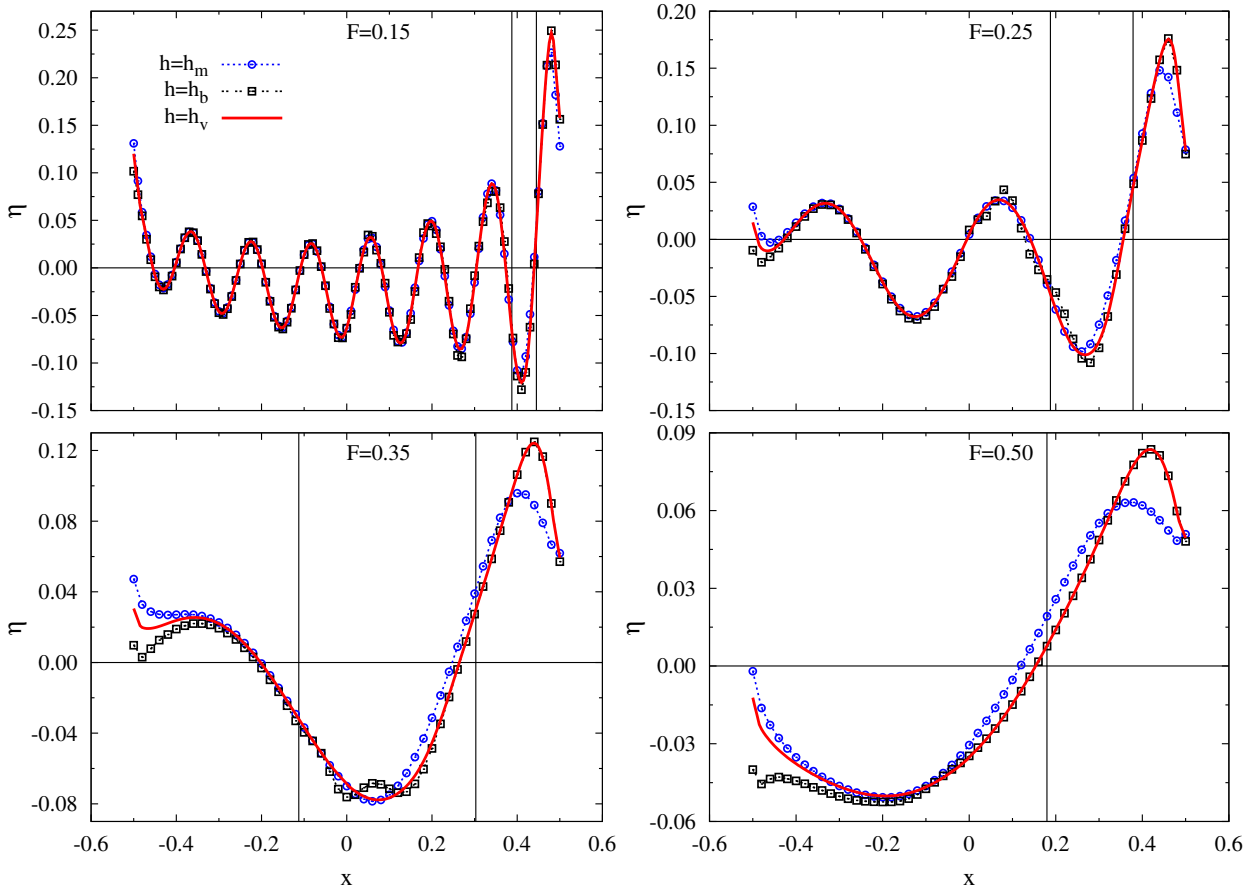

Figure 5: Wave profiles, predicted by Hogner's slender-ship approximation, along the Wigley hull at four Froude numbers $F = 0.15,\ 0.25,\ 0.35$ and 0.5. The curves marked $h = h_m$ or $h = h_b$ correspond to an extrapolation height $\widetilde{h}$ that is constant for $-0.5 \le \widetilde{x} \le 0.5$ and equal to the basic extrapolation heights h_m or h_b defined by (10a). The curves $h = h_v$ correspond to an extrapolation height $\widetilde{h}(\widetilde{x})$ that varies from the bow to the stern as defined by (14a)-(14d) with (10a) and (10b). The vertical lines mark the boundaries of the transition region defined by (14b).

$1/2 - \mu_b F^2/(1+F_{BD}) \le \widetilde{x} \le 1/2$. The parameter $0 < \mu_b$ controls the extent of the bow region where $B_b \approx 1$. We also impose $B_b \approx 0$ at a distance aft of the ship bow that is related to the distance between the ship stem and the intersection of the bow wave with the mean free surface. This distance (the length of the bow wave) is shown in [13] to be approximately given by $2.3F^2$. We then impose $B_b \approx 0$ for $\widetilde{x} \le 1/2 - \mu_m F^2$. The parameter $0 < \mu_m$ controls the extent of the region within which the function $B_b(\widetilde{x})$ is not approximately nil. Thus, the function $B_b(\widetilde{x})$ varies from 1 to 0, and the related extrapolation height $\widetilde{h}$ defined by (14a) varies from h_b to h_m, within the region

$$1/2 - \mu_m F^2 \le \widetilde{x} \le 1/2 - \mu_b F^2/(1+F_{BD}) \tag{14b}$$

The length $[\mu_m - \mu_b/(1+F_{BD})]F^2$ of this transition region is controlled by the parameters μ_b and μ_m, and is positive if $\mu_b/\mu_m < 1+F_{BD} \equiv 1+F/\sqrt{\sigma^H}$. The distance $\mu_m F^2$ related to the length of the bow wave is smaller or greater than 1 in the low or high Froude number regimes $F < 1/\sqrt{\mu_m}$ or $1/\sqrt{\mu_m} < F$, for which expression (14a) for h_{mb} yields $b_{mb} = h_m$ or $h_{mb} < h_m$, respectively. Values of μ_b and μ_m within the ranges $3 \le \mu_b \le 5$ and $4 \le \mu_m \le 6$ are reasonable. Numerical tests show that $\mu_b = 4$ and $\mu_m = 5$ are satisfactory choices. The choice $\mu_m = 5$ yields $1/\sqrt{\mu_m} = 1$ for $F \approx 0.45$. The functions $x^m \equiv \mu_m F^2$ and $x^b \equiv \mu_b F^2/(1+F_{BD})$ are depicted on the left side of Fig.4 for $\mu_m = 5$, $\mu_b = 4$ and $\sigma^H = 0.06$. We have

$$\frac{4F^2}{1+F_{BD}} < 1 \quad \text{for} \quad F < \frac{1+\sqrt{1+16\,\sigma^H}}{8\sqrt{\sigma^H}} \approx 1.2 \quad \text{if} \quad \sigma^H = 0.06$$

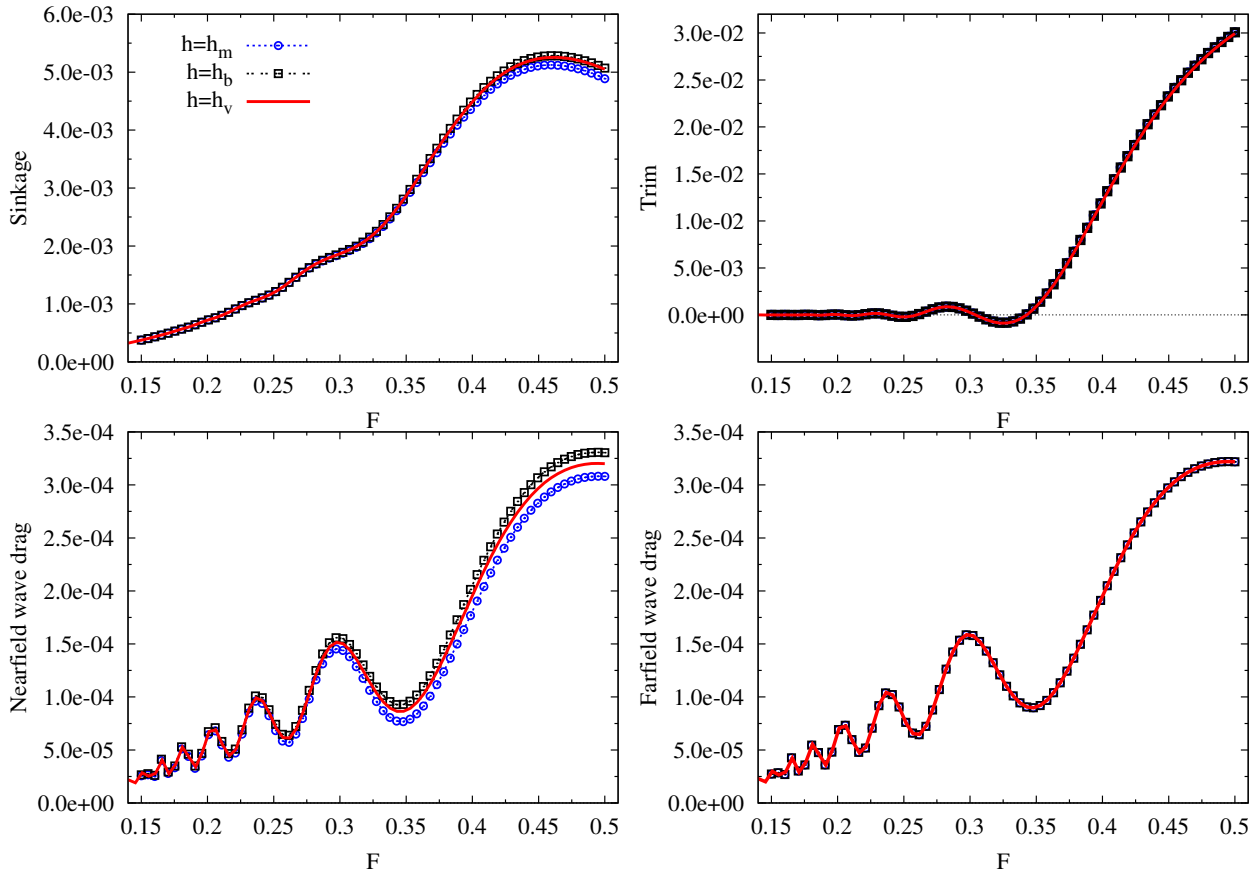

Figure 6: Sinkage (top left corner), trim (top right), nearfield drag (bottom left), farfield drag (bottom right) predicted by Hogner's slender-ship approximation for the Wigley hull in the range $0.15 \le F \le 0.5$. The curves marked $h = h_m$ or $h = h_b$ correspond to an extrapolation height $\widetilde{h}$ that is constant for $-0.5 \le \widetilde{x} \le 0.5$ and equal to the basic extrapolation heights h_m or h_b defined by (10a). The curves $h = h_v$ correspond to an extrapolation height $\widetilde{h}(\widetilde{x})$ that varies from the bow to the stern as defined by (14a)-(14d) with (10a) and (10b).

A continuous transition between h_b and h_m can be defined. For instance, the transition function

$$2\,B_b(\widetilde{x}) \equiv 1 + \tanh \frac{2\,\widetilde{x} - 1 + F^2[\,\mu_m + \mu_b/(1+F_{BD})\,]}{F^2[\,\mu_m - \mu_b/(1+F_{BD})\,]/2} \quad \text{with} \quad \frac{-1}{2} \le \widetilde{x} \le \frac{1}{2} \tag{14c}$$

and $\mu_b = 4$, $\mu_m = 5$ yields $B_b \approx 0.98$ for $\widetilde{x} = 1/2 - \mu_b F^2/(1+F_{BD})$ and $B_b \approx 0.02$ for $\widetilde{x} = 1/2 - \mu_m F^2$.

The function B_s associated with the decrease of the extrapolation height $\widetilde{h}$ near the ship stern is taken as

$$B_s(\widetilde{x}) \equiv e^{-4\,(\,\widetilde{x}\,+\,1/2\,)\,/\,\ell_s} \quad \text{with} \quad -1/2 \le \widetilde{x} \le 1/2 \tag{14d}$$

The parameter ℓ_s defines the stern region within which $\widetilde{h}$ may be decreased if the hull geometry changes rapidly. The value $\ell_s = 0.4$ is a reasonable choice and is used here.

The right side of Fig.4 depicts the variation of the extrapolation height $\widetilde{h}(\widetilde{x})$ defined by (14a)-(14d) with (10a) and (10b) for $F = 0.15$, 0.25, 0.35, 0.5 and $F_t = 0.4$, $\sigma^H = 0.06$, $\varepsilon_b = 0.04$, $\mu_b = 4$, $\mu_m = 5$, $\varepsilon_m = 0.06$, $C_s^m = 0.7$ and $\ell_s = 0.4$. In accordance with expressions (14a)-(14d), Fig.4 shows that the extrapolation height $\widetilde{h}(\widetilde{x})$ is smallest within the bow region, increases from the bow value $\widetilde{h} = h_b$ to the midship value $\widetilde{h} = h_m$ within the transition region (14b), and decreases from the midship value $\widetilde{h} = h_m$ to the stern value $\widetilde{h} = h_s$ near the stern $\widetilde{x} = -1/2$. Fig.4 also illustrates how the values h_b, h_m and h_s, and the extents of the bow-wave and midship regions, and of the transition region between these two regions, vary with the Froude number F.

For illustration purposes, the Hogner slender-ship approximation is considered again for the Wigley parabolic hull in Fig.5. This figure depicts the wave profiles along the Wigley hull for four Froude numbers $F = 0.15$, 0.25, 0.35 and 0.5. Three cases are considered in Fig.5. Two of the cases, marked $h = h_m$ or $h = h_b$, correspond to an extrapolation height $\widetilde{h}$ that is constant for $-0.5 \le \widetilde{x} \le 0.5$ and equal to the basic extrapolation

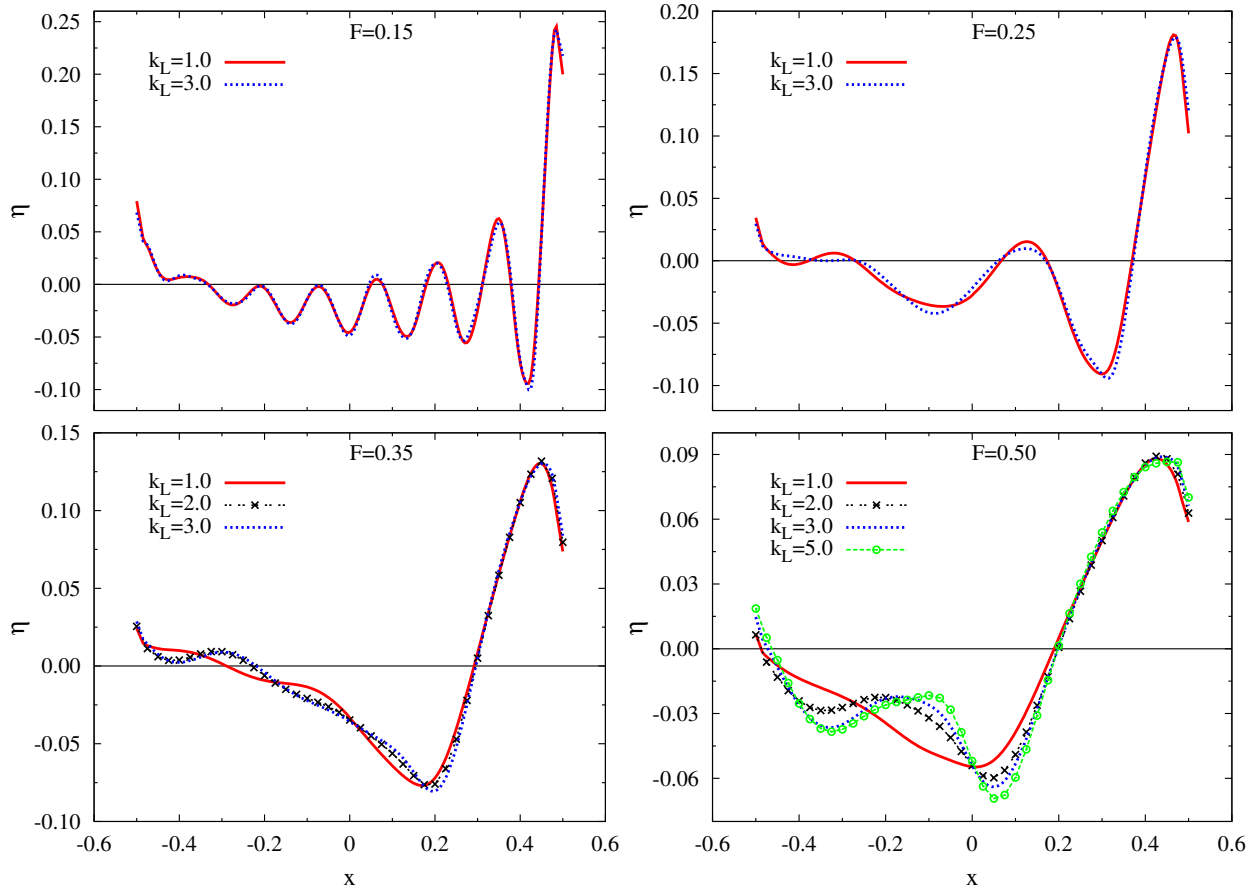

Figure 7: Wave profiles along the Wigley hull, at four Froude numbers $F = 0.15$, 0.25, 0.35, 0.5, predicted by the NM theory with several values of k_L.

heights h_m or h_b defined by (10a). The third case, marked $h = h_v$, corresponds to an extrapolation height $\widetilde{h}(\widetilde{x})$ that varies from the bow to the stern as defined by (14a)-(14d) with (10a) and (10b). The boundaries of the transition region defined by (14b) are marked by two vertical lines in Fig.5. The extent of the transition region increases as F increases, as already illustrated on the left side of Fig.4. For $F = 0.15$, the transition region is narrow, whereas only one vertical line appears in the bottom right corner of Fig.5 because the transition region extends beyond the ship stern $\widetilde{x} = -0.5$ for $F = 0.5$. In the bow region to the right of the transition region, the wave profiles $h = h_v$ and $h = h_b$ cannot be distinguished, and are appreciably higher than the profiles $h = h_m$ as already noted in Fig.2. To the left of the transition region, the profiles $h = h_v$ and $h = h_m$ are nearly identical, except near the stern $\widetilde{x} = -0.5$ where the wave profiles $h = h_v$ are lower than the profiles $h = h_m$ in accordance with (10b). Within the transition regions marked by vertical lines in Fig.5, the wave profiles $h = h_v$ smoothly merge between the profiles $h = h_b$ and the profiles $h = h_m$ as expected from (14a).

Fig.6 shows the sinkage (top left corner), the trim (top right), and the nearfield (bottom left) and farfield (bottom right) wave drags — predicted by the Hogner approximation for the Wigley hull — that correspond to the wave profiles shown in Fig.5. In accordance with Fig.3, the curves $h = h_m$, $h = h_b$ and $h = h_v$ can hardly be distinguished for the trim and the farfield wave drag, and differences are relatively small for the nearfield drag and, especially, the sinkage. In particular, the curves $h = h_v$ are $h = h_b$ are quite close, especially at low Froude numbers and for the sinkage.

5 Neumann-Michell theory

The Neumann-Michell (NM) theory of ship waves given in [3] expresses the amplitude A of the elementary wave E in the wave-spectrum function (3) as the Hogner amplitude $A = A^H$ given by (4) and a correction A^ψ. Specifically, the NM amplitude function is given by

$$A = A^{NM} \equiv A^H + A^\psi \quad \text{with} \quad A^\psi \equiv (k\,\nu^y + i\sqrt{1+k^2}\,\nu^z)\,\phi_t + n^x(k\,\nu^z - i\sqrt{1+k^2}\,\nu^y)\,\phi_d \tag{15}$$

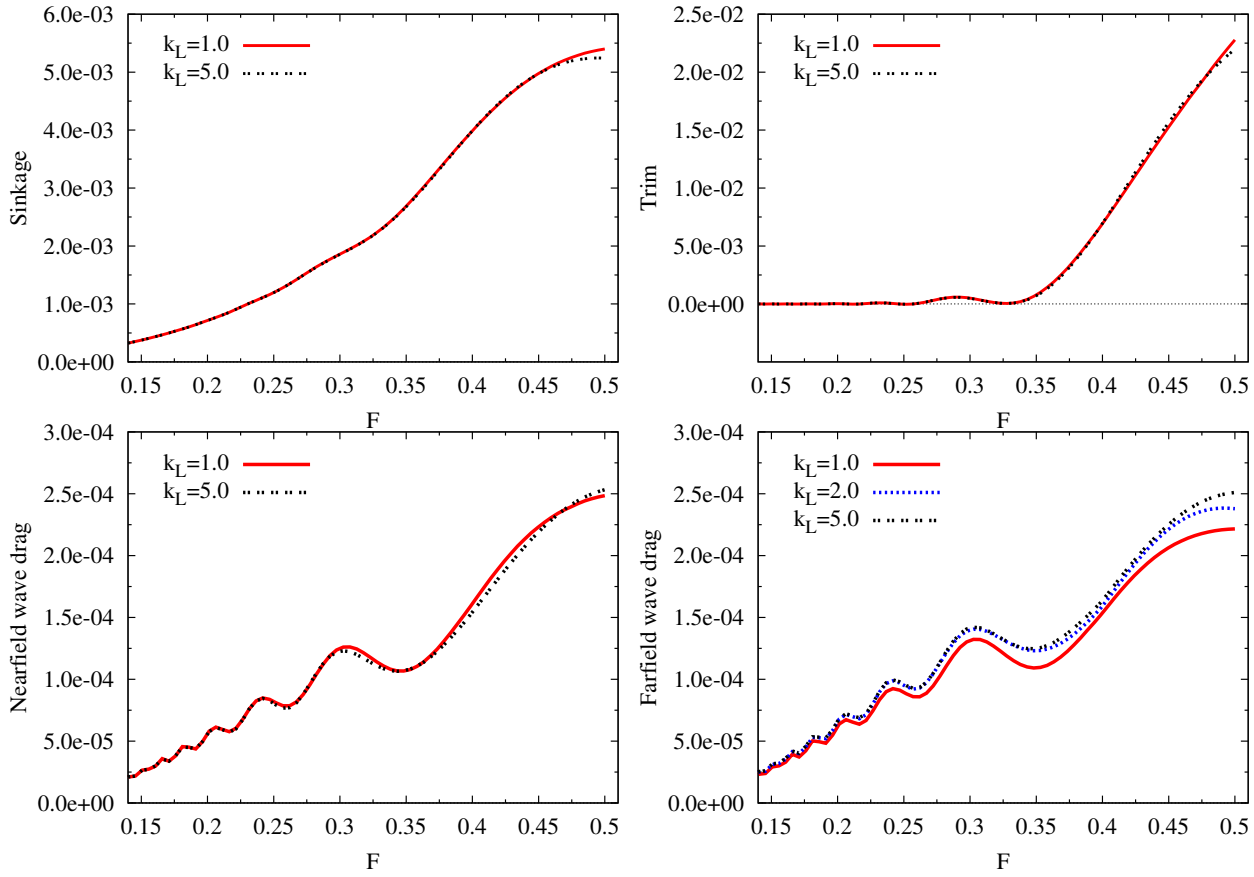

Figure 8: Sinkage (top left corner), trim (top right), nearfield drag (bottom left), farfield drag (bottom right) for the Wigley hull, in the range $0.15 \leq F \leq 0.5$, predicted by the NM theory with several values of k_L.

Here, $(\nu^y, \nu^z) \equiv (n^y, n^z)/\nu$ with $\nu \equiv \sqrt{(n^y)^2 + (n^z)^2}$. Furthermore, $\phi_d \equiv \partial\phi/\partial d$ and $\phi_t \equiv \partial\phi/\partial t$ are the flow velocities along the orthogonal unit vectors $\mathbf{d} \equiv (0, -\nu^z, \nu^y)$ and $\mathbf{t} \equiv (\nu, -n^x\nu^y, -n^x\nu^z)$. The unit vectors $\mathbf{d}$ and $\mathbf{t}$ are tangent to the ship hull surface Σ^H. The unit vector $\mathbf{d}$ points upward on the positive side of Σ^H, where $0 < y$ and $0 < n^y$, or downward on the negative side of Σ^H where $y < 0$ and $n^y < 0$. The unit vector $\mathbf{t}$ points toward the ship bow on both sides of the hull surface Σ^H.

The Hogner amplitude $A^H \equiv n^x$ is independent of k and consequently does not grow as $k \to \pm\infty$. However, the amplitude function A^ψ of the NM correction is $O(k)$ as $k \to \pm\infty$. The NM wave potential associated with the amplitude function A^ψ in the wave-spectrum function $\widetilde{S}$ is then influenced by short waves to a greater extent than the Hogner wave potential associated with the amplitude function A^H. The short-wave content of the NM wave correction potential can be attenuated by replacing k in (15) by the function k_* defined as

$$k_* \equiv k \ \text{ for } \ -k_L \leq k \leq k_L \qquad k_* \equiv k_L \,\text{sign}(k) \ \text{ for } \ k_L < |k| \tag{16}$$

This modification does not affect long waves associated with the range $-k_L \leq k \leq k_L$ but affects short waves outside this long-wave range.

Fig.7 shows the wave profiles along the Wigley hull, at $F = 0.15$, 0.25, 0.35 and 0.5, predicted by the NM theory with several values of k_L. The wave profiles obtained for $k_L = 1$ and 3 cannot be distinguished for $F = 0.15$ and are fairly close for $F = 0.25$. For $F = 0.35$, the wave profiles for $k_L = 2$ and 3 can hardly be distinguished, but these profiles differ appreciably from the profile obtained for $k_L = 1$. For $F = 0.5$, the wave profiles are significantly influenced by k_L. In particular, the wave profile $k_L = 1$ is significantly less oscillatory than the profiles $k_L = 2$, 3 and 5. The increasing effect of k_L for larger Froude numbers illustrated in Fig.7 is consistent with Fig.1, which shows that short waves become increasingly more important as the Froude number increases. Fig.8 shows that differences in the sinkage, trim and nearfield drag obtained for $k_L = 1$ and $k_L = 5$ are small. The farfield drag obtained for $k_L = 1$ is appreciably lower, especially at high Froude numbers, than the drags obtained for $k_L = 2$ or 5, which are relatively close. Fig.8 and Fig.7 suggest that the physically reasonable choice $k_L = 2$, which means that waves with wavelength $\lambda_0/5 \leq \lambda \leq \lambda_0$ are unaffected by the modification (16), is satisfactory, and this choice is used here.

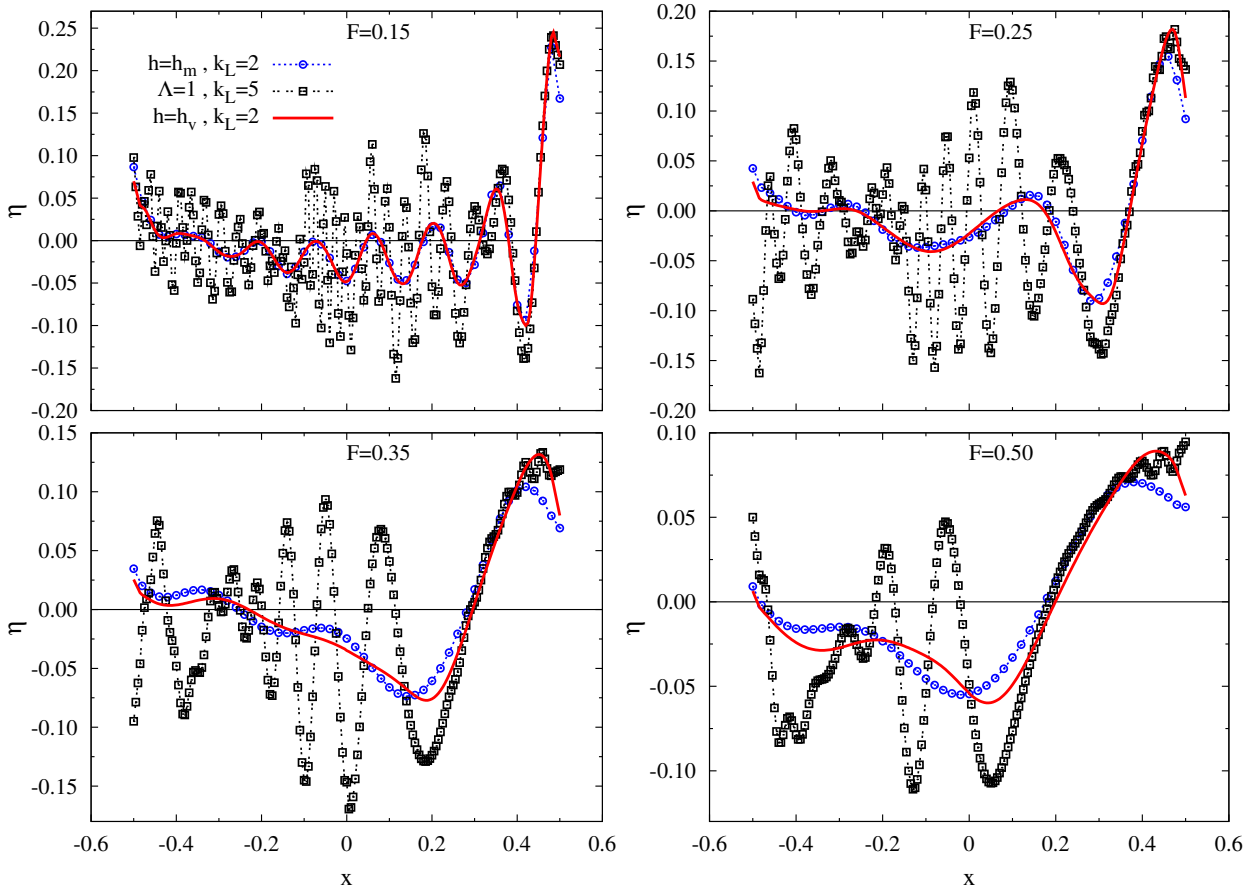

Figure 9: Wave profiles, predicted by the NM theory, along the Wigley hull at four Froude numbers $F = 0.15$, 0.25, 0.35 and 0.5. The curves marked $h = h_m$, $k_L = 2$ correspond to an extrapolation height $\widetilde{h}$ that is constant for $-0.5 \le \widetilde{x} \le 0.5$ and equal to the midship extrapolation height h_m given by (10a). The curves marked $h = h_v$, $k_L = 2$ correspond to an extrapolation height $\widetilde{h}(\widetilde{x})$ that varies from the bow to the stern as specified by (14a)-(14d) with (10a) and (10b). The value of k_L in (16) is taken equal to 2 for the curves marked $h = h_m$, $k_L = 2$ or $h = h_v$, $k_L = 2$. The curves marked $\Lambda = 1$, $k_L = 5$ correspond to $k_L = 5$, $\Lambda = 1$ (no parabolic filter) and k_∞ given by (11) in (7), i.e. short waves are not filtered in the curves $\Lambda = 1$, $k_L = 5$.

The need for filtering short waves is further illustrated in Fig.9, which shows wave profiles predicted by the NM theory along the Wigley hull at four Froude numbers $F = 0.15$, 0.25, 0.35 and 0.5, and in Fig.10 which depicts the sinkage (top left corner), trim (top right), nearfield drag (bottom left) and farfield drag (bottom right) predicted by the NM theory for the Wigley hull in the range $0.15 \le F \le 0.5$. Three cases are considered in these two figures. The curves marked $h = h_m$, $k_L = 2$ correspond to an extrapolation height $\widetilde{h}$ that is constant for $-0.5 \le \widetilde{x} \le 0.5$ and equal to the midship extrapolation height h_m given by (10a). The curves marked $h = h_v$, $k_L = 2$ correspond to an extrapolation height $\widetilde{h}(\widetilde{x})$ that varies from the bow to the stern in accordance with (14a)-(14d) with (10a) and (10b). The value of k_L in (16) is taken equal to 2 for the curves marked $h = h_m$, $k_L = 2$ or $h = h_v$, $k_L = 2$. The main difference between the curves $h = h_m$ and $h = h_v$ is that the short waves contained in the bow wave are included in the curves $h = h_v$ but are ignored in the curves $h = h_m$. The curves marked $\Lambda = 1$, $k_L = 5$ correspond to $k_L = 5$, $\Lambda = 1$ (no parabolic filter) and k_∞ given by (11) in (7). Thus, short waves are not filtered in the curves $\Lambda = 1$, $k_L = 5$. Fig.9 shows that the wave profiles $\Lambda = 1$, $k_L = 5$ contain large unrealistic oscillations, especially aft of the bow wave, and that the wave profiles $h = h_m$, $k_L = 2$ exhibit overly damped bow waves, notably for $F = 0.35$ and 0.40. Fig.10 shows that differences in the sinkage, trim and wave drag associated with the alternative choices $h = h_m$ or $h = h_v$ are appreciable for the wave drag, but insignificant for the sinkage and trim. The 'no-filtering' choice $\Lambda = 1$ and $k_L = 5$ yields overly oscillatory wave-drag curves that are significantly different from the curves $h = h_m$ or $h = h_v$.

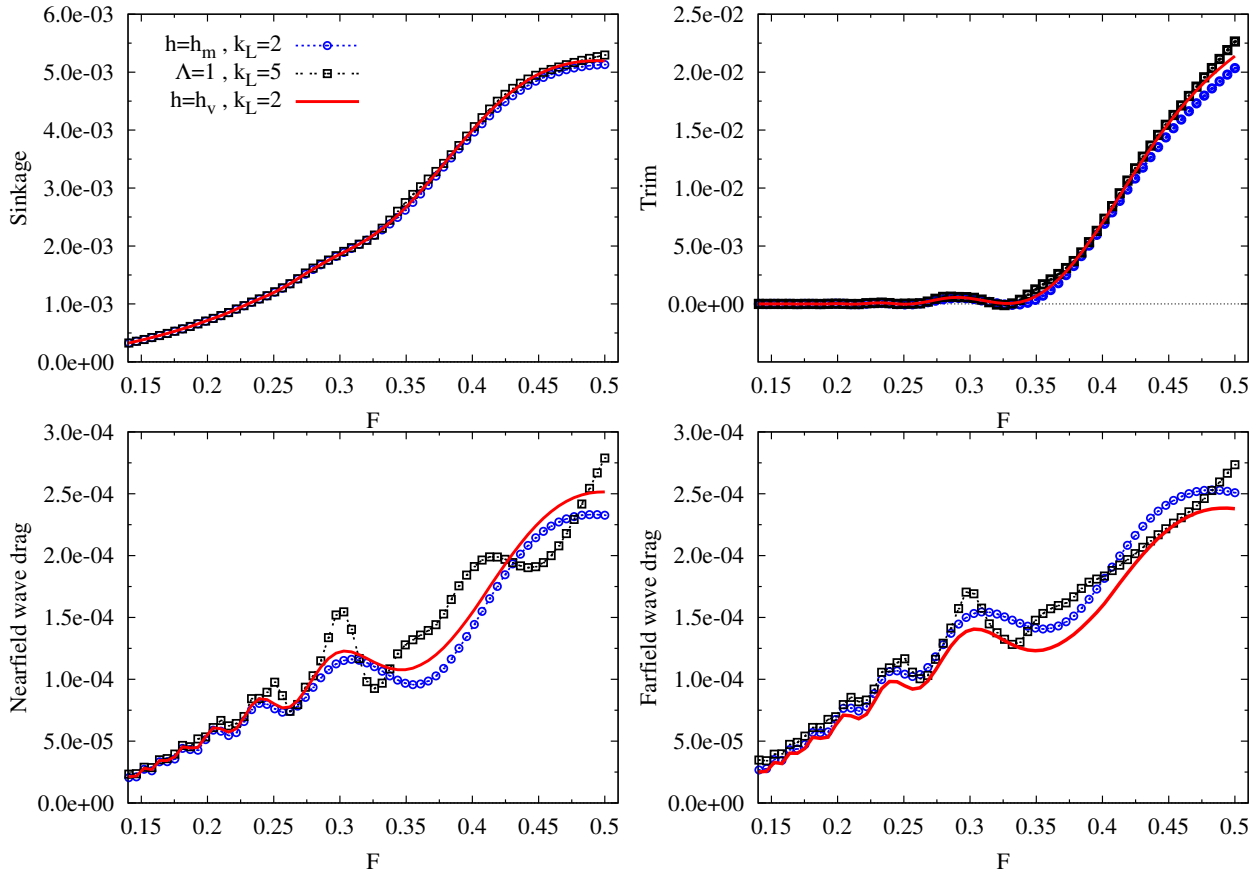

Figure 10: Sinkage (top left corner), trim (top right), nearfield drag (bottom left), farfield drag (bottom right) predicted by the NM theory for the Wigley hull in the range $0.15 \leq F \leq 0.5$. The curves marked $h = h_m$, $k_L = 2$ correspond to an extrapolation height $\widetilde{h}$ that is constant for $-0.5 \leq \widetilde{x} \leq 0.5$ and equal to the midship extrapolation height h_m given by (10a). The curves marked $h = h_v$, $k_L = 2$ correspond to an extrapolation height $\widetilde{h}(\widetilde{x})$ that varies from the bow to the stern as specified by (14a)-(14d) with (10a) and (10b). The value of k_L in (16) is taken equal to 2 for the curves marked $h = h_m$, $k_L = 2$ or $h = h_v$, $k_L = 2$. The curves marked $\Lambda = 1$, $k_L = 5$ correspond to $k_L = 5$, $\Lambda = 1$ (no parabolic filter) and k_∞ given by (11) in (7), i.e. short waves are not filtered in the curves $\Lambda = 1$, $k_L = 5$.

6 Conclusion

A reasonable and practical approach, based on parabolic extrapolation within a layer bordering the mean free-surface plane $z = 0$, for evaluating waves in the vicinity of the plane $z = 0$ within the framework of the 'free-surface Green function potential flow theory' (based on a Green function that satisfies the radiation condition and the Kelvin-Michell linearized boundary condition at the free surface) has been given. This parabolic-extrapolation approach effectively filters short waves, as illustrated in Fig.2 and Fig.9. The reported analysis and illustrative calculations confirm the (well-understood) need for removing ship waves that are short in comparison to the ship length, or that may be so short as to be affected by surface tension or viscosity, and consequently are not relevant in practice or indeed physically unrealistic.

The short-wave filter based on parabolic extrapolation amounts to modifying the basic Fourier representation (2) of ship waves as in (7). The filter function Λ in the modified Fourier representation (7) is given by (8) for the parabolic extrapolation considered here. The height $\widetilde{h}$ of the extrapolation layer associated with the filter function Λ depends on the Froude number and the slenderness of the ship hull, and varies from the ship bow to the ship stern, as illustrated in Fig.4. This bow-to-stern variation accounts for the fact that waves along the ship hull aft of the bow wave differ from the bow wave. Indeed, the bow wave is significantly higher, shorter and therefore steeper than waves aft of the bow wave, is significantly affected by nearfield effects related to the rapid variation of the hull geometry at a ship bow, and consequently contains more short wave components. The extrapolation height $\widetilde{h}$ is determined explicitly, by means of expressions (14) and (10), in terms of the Froude number F, the slenderness σ^H of the ship hull, and the location $\widetilde{x}$

along the ship waterline. These expressions involve six parameters that have a clear physical meaning. The Neumann-Michell correction to the Hogner slender-ship approximation involves an additional parameter that restricts the influence of divergent waves and also has a physical significance. Numerical predictions, notably of the sinkage, trim and wave drag, are not overly sensitive to the values chosen for these seven parameters associated with the short-wave filter considered here.

Comparisons between experimental measurements and numerical predictions given by the NM theory or the related Hogner slender-ship approximation with the short-wave filter defined by (8), (10), (14), (16) and

$$\epsilon_b = 0.04 \qquad \mu_b = 4 \qquad \mu_m = 5 \qquad \epsilon_m = 0.06 \qquad C_s^m = 0.7 \qquad \ell_s = 0.4 \qquad k_L = 2$$

are reported in [15] for the classic Wigley parabolic hull and Series 60 model .

Acknowledgments

This work was funded by the Naval Surface Warfare Center, Carderock Division, and the Office of Naval Research. We warmly thank Ms. Kelly Cooper for her interest and support.

References

[1] Noblesse F (1981) Alternative integral representations for the Green function of the theory of ship wave resistance. J Eng Math 15:241-265
[2] Noblesse F, Delhommeau G, Huang F, Yang C (2011) Practical mathematical representation of the flow due to a distribution of sources on a steadily-advancing ship hull. J Eng Math 71:367-392
[3] Noblesse F, Huang F, Yang C (2012) The Neumann-Michell theory of ship waves, J Eng Math, in press
[4] Hogner E (1932) Hydromech. Probl. d. Schiffsantriebs, Herausgeg.v.Kempf u. E. Foerster, Hamburg 99-114
[5] Noblesse F, Yang C (2007) Elementary water waves, J Eng Math 59:277-299
[6] Chen XB & Dias F (2010) Visco-potential flow and time-harmonic ship waves. 25th Il Workshop on Water Waves & Floating Bodies, Harbin, China
[7] Chen X.B. & Lu D.Q. (2009) Time-harmonic ship waves with the effect of surface tension and fluid viscosity. 24th IWWWFB, Zelenogork, Russia
[8] Dias F, Dyachenko AI & Zakharov VE (2008) Theory of weakly damped free-surface flows: A new formulation based on potential flow solutions. Physics letters, A, 1297-1302
[9] Dutykh D & Dias F (2007) Viscous potential free-surface flows in a fluid layer of finite depth. C.R. Acad. Sci. Paris, Ser. I, 345, 113-118
[10] Noblesse F, Delhommeau G, Huang F & Yang C (2011) Short gravity waves due to a steadily-advancing ship hull. 26th Il Workshop on Water Waves & Floating Bodies, Athens, Greece
[11] Noblesse F, Delhommeau G, Guilbaud M, Hendrix D, Yang C (2008) Simple analytical relations for ship bow waves. J Fluid Mechanics 600:105-132
[12] Shakeri M, Tavakolinejad M, Duncan, JH (2009) An experimental investigation of divergent bow waves simulated by a two-dimensional plus temporal wavemaker technique, J Fluid Mechanics 634: 217- 243
[13] Noblesse F, Delhommeau G, Yang C, Kim HY, Queutey P (2011) Analytical bow waves for fine ship bows with rake and flare. J Ship Res 55:1-18
[14] Delhommeau G, Guilbaud M, David L, Yang C, Noblesse F (2009) Boundary between unsteady and overturning ship bow wave regimes. Jl Fluid Mechanics 620:167-175
[15] Noblesse F, Huang F, Yang C (2012) Evaluation of ship waves at the free surface and removal of short waves. Submitted.